npj | Quantum Materials

www.nature.com/npjquantmats

ARTICLE OPEN

Negative thermal expansion in $YbMn_2Ge_2$ induced by the dual effect of magnetism and valence transition

Yongqiang Qiao[1], Yuzhu Song[1], Andrea Sanson[2], Longlong Fan[3], Qiang Sun[4], Shuxian Hu[5], Lunhua He[6], Hongjie Zhang[7], Xianran Xing[8] and Jun Chen[1,5]✉

Negative thermal expansion (NTE) is an intriguing property, which is generally triggered by a single NTE mechanism. In this work, an enhanced NTE ($\alpha_v = -32.9 \times 10^{-6}\ K^{-1}$, $\Delta T = 175$ K) is achieved in $YbMn_2Ge_2$ intermetallic compound to be caused by a dual effect of magnetism and valence transition. In $YbMn_2Ge_2$, the Mn sublattice that forms the antiferromagnetic structure induces the magnetovolume effect, which contributes to the NTE below the Néel temperature (525 K). Concomitantly, the valence state of Yb increases from 2.40 to 2.82 in the temperature range of 300–700 K, which simultaneously causes the contraction of the unit cell volume due to smaller volume of Yb^{3+} than that of Yb^{2+}. As a result, such combined effect gives rise to an enhanced NTE. The present study not only sheds light on the peculiar NTE mechanism of $YbMn_2Ge_2$, but also indicates the dual effect as a possible promising method to produce enhanced NTE materials.

npj Quantum Materials (2021)6:49 ; https://doi.org/10.1038/s41535-021-00348-z

INTRODUCTION

Positive thermal expansion (PTE) is a common property of materials, which is caused by anharmonic thermal vibrations between atoms. Differently, negative thermal expansion (NTE) exhibiting as an unusual property has been received wide attention in the last two decades. Various interesting NTE materials are known to date, such as oxides[1–5], intermetallic compounds[6,7], fluorides[8,9], cyanides[10–12], and nitrides[13,14]. The discovery of NTE materials opens up the possibility to control the thermal expansion for high precision applications such as microelectronic devices, optical mirrors, micromechanics, and so on.

In the study of NTE materials, various kinds of mechanisms have been found out. In general, the NTE mechanisms can be divided into two categories: one is electron-driven type, such as valence transition[15–18], magnetovolume effect (MVE)[6,7,13,19,20] and spontaneous volume ferroelectrostriction (SVFS)[21]; the second is phonon-mediated type, such as rigid unit modes (RUMs)[22,23] and guitar-string effect[9,24]. On the basis of these mechanisms, the methods of chemical substitution[2,25], nanocrystallization[26,27], guest ions or molecular intercalation[12,28], and other methods have been tried to regulate NTE. Actually, most of these methods weaken the NTE properties, scilicet the magnitude and the temperature range of the NTE. As a result, it is not easy to enhance NTE properties. Considering the fact that there is no inherent contradiction among the above NTE mechanisms, the combination of two of these mechanisms could help to improve NTE in magnitude and temperature range through a dual effect.

As a ternary rare-earth RT_2X_2 compounds (where R is a rare earth metal, T is a 3d or 4d transition metal, and X is silicon or germanium), it is interesting to observe that the a-axis of $YbMn_2Ge_2$ exhibits the NTE phenomenon[29,30], which is rare in the RT_2X_2 compounds. In such temperature region, the magnetic structure undergoes a transition from antiferromagnetism to paramagnetism[31], and the valence state of Yb shows a temperature-dependent behavior[29]. As we know, the magnetic transition may bring about the magnetovolume effect[6,7,13,19,20], and the valence transition can also give a volume change[15–18]. Therefore, $YbMn_2Ge_2$ is a good candidate for studying the dual effect on thermal expansion. In the present study, the NTE behavior of $YbMn_2Ge_2$ has been systematically investigated by means of synchrotron X-ray diffraction (SXRD). The combined analysis of neutron powder diffraction (NPD) and X-ray absorption near edge structure (XANES) reveals the clear relationship between the dual effect and the NTE in $YbMn_2Ge_2$. The dual effect, due to the spontaneous volume magnetostriction induced by Mn moment and to the valence transition by Yb atoms, gives rise to enhanced NTE, both in magnitude and temperature range. This work enables us to have a deeper understanding of the NTE mechanism in the specific case of $YbMn_2Ge_2$ and, above all, provides an idea to obtain interesting NTE materials by exploiting the dual effect from the well-known NTE mechanisms.

RESULTS AND DISCUSSION

Enhanced negative thermal expansion

Temperature dependent SXRD measurements of $YbMn_2Ge_2$ were performed to obtain accurate crystal structure information and lattice parameters (Supplementary Fig. 1). The Rietveld method was adopted to refine the crystal structure, which revealed a good agreement with the $I4/mmm$ space group (Supplementary Fig. 2a). As shown in Fig. 1a, the Yb, Mn, and Ge atoms occupy the Wyckoff sites 2a (0, 0, 0), 4d (0, 0.5, 0.25), and 4e (0, 0, z), respectively. They stack with the sequence of Yb-Ge-Mn-Ge-Yb along the c-axis. The

[1]Beijing Advanced Innovation Center for Materials Genome Engineering, and Department of Physical Chemistry, University of Science and Technology Beijing, Beijing, China. [2]Department of Physics and Astronomy, University of Padova, Padova, Italy. [3]College of Physics and Materials Science, Tianjin Normal University, Tianjin, China. [4]International Laboratory for Quantum Functional Materials of Henan, School of Physics and Engineering, Zhengzhou University, Zhengzhou, China. [5]School of Mathematics and Physics, University of Science and Technology Beijing, Beijing, China. [6]Institute of Physics, Chinese Academy of Sciences, Beijing, China. [7]Department of Chemistry, Tsinghua University, Beijing, China. [8]Beijing Advanced Innovation Center for Materials Genome Engineering, and Institute of Solid-State Chemistry, University of Science and Technology Beijing, Beijing, China. ✉email: junchen@ustb.edu.cn

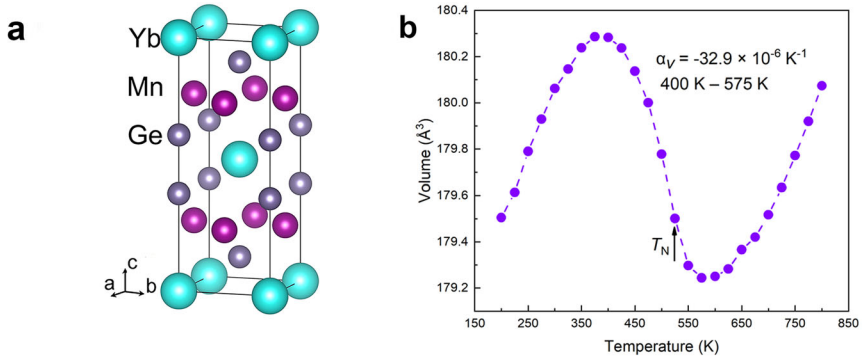

Fig. 1 Crystal structure and thermal expansion characteristics. a Crystal structure of $YbMn_2Ge_2$, and **b** temperature dependence of the unit cell volume.

temperature dependence of the lattice parameters is plotted in Supplementary Fig. 2b. It can be observed that *a*-axis shows a strong NTE while *c*-axis shows a normal positive thermal expansion, which is consistent with the previous literature studies[30]. Combining the lattice parameters of *a* and *c*, the unit cell volume can be calculated (Fig. 1b). Interestingly, a NTE is observed in the unit cell volume over a relatively wide temperature ($\alpha_v = -32.9 \times 10^{-6}\,K^{-1}$, 400–575 K, $\Delta T = 175$ K).

Magnetic structure

Note that such NTE over a relative wide temperature range is rare in ternary rare-earth RT_2X_2 compounds[32,33]. Accordingly, it is of great scientific significance to study the NTE mechanism in the present $YbMn_2Ge_2$. It is well known that MVE is the key factor for the NTE behavior happening in the magnetic NTE compounds such as the Invar alloys, the prototype magnetic NTE materials discovered by C. É Guillaume[34]. Herein, the detailed magnetic information has been extracted from the NPD measurements collected in the temperature range 35–615 K (Supplementary Fig. 3). Considering the influence of magnetism on the diffraction patterns, the pattern at 600 K was used as the refinement for the non-magnetic state. As mentioned in the experimental part, an aluminum foil was wrapped outside the vanadium cans for a better temperature management. Therefore, two phases of $YbMn_2Ge_2$ and Al were used to refine the pattern at 600 K. The calculated pattern is in a good agreement with the predominant reflections. A few fractions of impurities can be discerned (Supplementary Fig. 4), as often happens in the preparation of Yb-containing compounds[35,36].

As observed from the temperature-dependent NPD patterns, some diffraction peaks change significantly with temperature (Supplementary Fig. 5). Based on comprehensive research on the magnetic structure of the RT_2X_2 series compounds, it is possible to evaluate the magnetic structure from the temperature dependence of some key indicators in the NPD patterns, such as the (101) and (103) reflections[37–39]. It can be seen that the integrated intensities of the two reflections have the same trend (Fig. 2a), which decreases with increasing temperature, reaching the minimum value at 525 K. Such threshold temperature is well consistent with the in-plane antiferromagnetic structure (AF*I*) transition point T_N (~510 K)[31,40,41]. Furthermore, the (111) reflection is observed below 300 K, which means that the Mn sublattice has an interlayer antiferromagnetic component superimposed on the in-plane antiferromagnetism, prompting the formation of another antiferromagnetic structure called AF*mc*[41]. The above two magnetic structures were respectively applied to the refinement of NPD data in different temperature regions (Supplementary Fig. 6). It can be seen that the calculated results and the experimental data are well matched regardless of peak position or intensity.

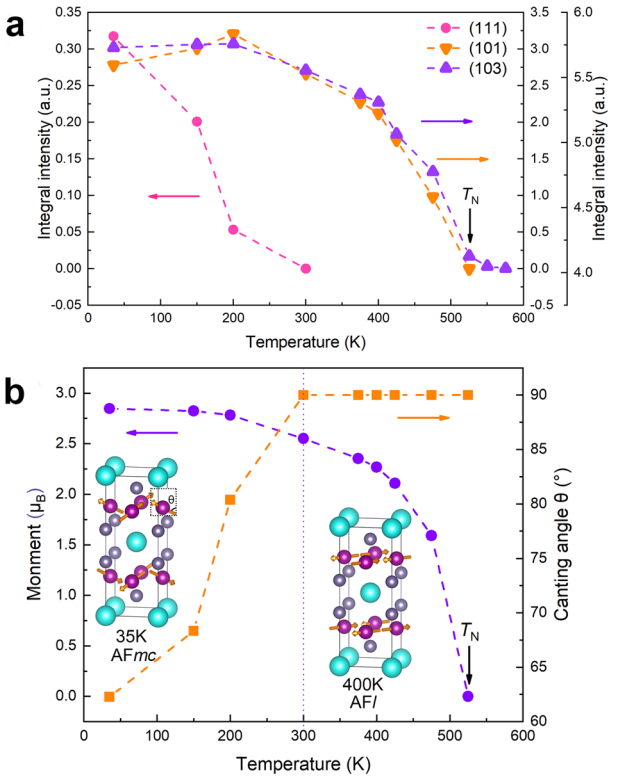

Fig. 2 Evolution of magnetic structure. Temperature dependence of **a** the integrated intensity of (101), (103), and (111) reflections, and **b** the magnetic moment and the canting angle, *θ*, of Mn atoms. The insets show the two antiferromagnetic structures of AF*mc* and AF*I*.

The schematic diagrams of two magnetic structures (AF*mc* and AF*I*) are shown in Fig. 2b. The angle (*θ*) between the direction of the Mn magnetic moment and the *c*-axis increases from 62° at 35 K to 90° at 300 K, which represents the transition of magnetic structure from AF*mc* to AF*I*. From the dependence on temperature of Mn magnetic moment (Fig. 2b), it can be observed that the magnetic moment slightly decreases with increasing temperature at the beginning, with a small effect on the unit cell volume. With further increasing temperature, the magnetic moment decreases more rapidly when approaching the magnetic transition temperature. Such dramatic change of the magnetic moment brings a negative effect on the thermal expansion, namely MVE, which can be quantitatively described by the spontaneous volume magnetostriction. However, from the comparison between Figs. 1b and 2b, it is interesting to observe that there is a large discrepancy

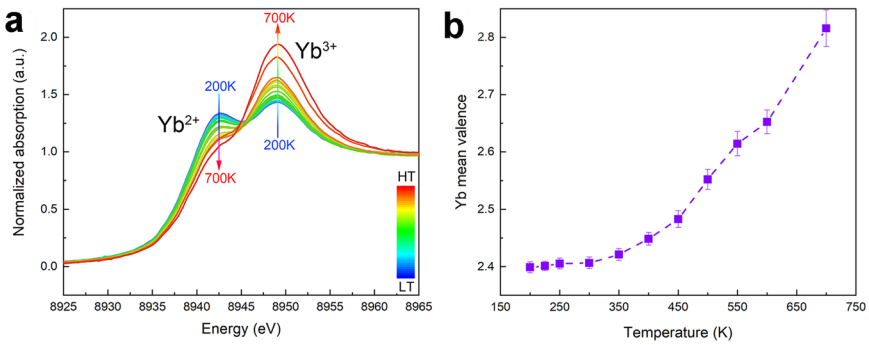

Fig. 3 The valence state characters of Yb. Temperature dependence of **a** the Yb L_{III}-edge XANES spectra, and **b** the valence state of Yb in $YbMn_2Ge_2$. Error bars represent confidence intervals of valence state.

between the temperatures where NTE and antiferromagnetic state disappear. NTE still persists in the paramagnetic state. Furthermore, the coefficient of thermal expansion between 575 K and 700 K is obviously lower than that above 700 K (Fig. 1b), which means that something else has to contribute to the NTE besides the MVE.

Temperature dependence of valence state

It is known that Yb can show two electronic configurations, Yb^{2+} ($4f^{14}5d^06s^2$) and Yb^{3+} ($4f^{13}5d^16s^2$)[42]. Because the energy difference between these two valence states is very small, external perturbations can easily cause changes between the two valence states[43]. As a result, the lattice parameters change since the atomic volume of Yb^{2+} (radius 1.16 Å) is larger than that of the Yb^{3+} (radius 1.01 Å)[44]. Therefore, the change of Yb valence state with temperature can be the phenomenon that further enhances the NTE behavior of $YbMn_2Ge_2$. To verify this, a XANES study as a function of temperature has been performed to determine the valence state of Yb in $YbMn_2Ge_2$. The collected Yb L_{III}-edge XANES spectra are shown in Fig. 3a. The first peak on the left at ~8943 eV is related to the presence of divalent Yb, while the second peak at ~8949 eV is related to the trivalent Yb[45,46]. It can be clearly seen that the peak intensity of divalent Yb is reduced by increasing temperature, while that of trivalent is enhanced. Two sets of functions are used to fit the data, which include a Lorentz and an arctangent function (Supplementary Fig. 7). The valence state can be so estimated by the integrated intensities of divalent and trivalent peaks[45]. As shown in Fig. 3b, the valence state of Yb is ~2.40 at low temperature, and remains almost unchanged between 200 K and 300 K, which is similar to the results in the literature[29]. Above 300 K, the valence state gradually increases with increasing temperature. Since there is a volume difference between Yb^{2+} and Yb^{3+} as mentioned above, not only the *a*-axis[29,30] but also the unit cell volume shows NTE due to the change in the valence state. At 700 K, the value rises to ~2.82. One needs to note the fact that the valence state of Yb in $YbMn_2Ge_2$ can quickly rise to 2.78 under a relatively small compressive pressure of 1.4 GPa, but only a small increase of 0.13 in the valence can be reached when the pressure is further enhanced to 10 GPa[47]. Therefore, it is reasonable to believe that the valence state of 2.82 at 700 K is close to its maximum limit in the present temperature dependence of valence transition. The $T_{valen.}$ at ~700 K can be assumed as the end temperature of valence transition.

The dual effect

To understand more in detail the origin of the enhanced NTE in $YbMn_2Ge_2$, one needs firstly to subtract the contribution of phonon vibrations to thermal expansion. Using the data of unit cell volume between 750–800 K which is far away from the effects of magnetism and valence transition, the contribution from phonon vibrations to the nominal thermal expansion (V_{nm}) is tentatively estimated according to the Debye-Grüneisen model[48,49]. As shown in Fig. 4a, it is interesting to find that the difference between the experimental volumes (V_{exp}) and the V_{nm} is still pronounced above the temperature of magnetic transition ($T_N = 525$ K). It is worth noting that such anomaly exists until 700 K, which is well consistent with the temperature for the end of valence transition. Therefore, not only magnetism but also valence transition contributes to the NTE of $YbMn_2Ge_2$, which can be called the dual effect. In order to try to isolate the contribution of valence transition from that of MVE, the difference (ΔV_{tol}) between V_{exp} and V_{nm} is plotted as a function of valence state of Yb (Fig. 4b). Since the T_N is at 525 K, we can use the valence value in the temperature range of 575–700 K, which is well above the T_N, to safely fit the contribution of valence transition to the NTE without the contribution from the MVE. As expected, the relationship between valence state and volume change is linear[50], and the line shown in Fig. 4b represents the contribution from the valence change, namely $\Delta V_{valen.}$. Then the contribution from MVE can be determined by the spontaneous volume magnetostriction using the equation of $\omega_{magn.} = (\Delta V_{tol.} - \Delta V_{valen.})/V_{nm}$. As shown in Fig. 4c, it is interesting to find a good correlation between $\omega_{magn.}$ and the square of Mn magnetic moment (M^2), which generally takes place in magnetic NTE materials[51,52]. Therefore, through the above analysis, the contributions of MVE and valence transition to NTE can be separated. As shown in Fig. 4d, the purple area represents the contribution from MVE, while the orange one stands for the contribution from valence change. Considering the $\omega_{magn.}$ in $YbMn_2Ge_2$, the value of 1.3% has the same order of magnitude of the values in magnetic NTE materials, such as 0.7–1.4% for Mn_3AN[53]. For the value of $\omega_{valen.}$ related to the valence transition, this is equal to 0.5%, comparable to the values of 0.9% in $Yb_{0.4}In_{0.6}Cu_2$[54] and 0.6% in $YbIn_{0.75}Ag_{0.25}Cu_4$[50]. Figure 4d gives a vision of the enhanced NTE in $YbMn_2Ge_2$ due to the dual effect of MVE and valence transition.

In the RT_2X_2 compounds, no magnetic moment has been found in the *T* site except for Mn atom[55–57]. Therefore, to better understand the enhanced NTE resulted from the dual effect, the thermal expansion of $YbFe_2Ge_2$ without magnetovolume effect has been studied for comparison. As shown in Supplementary Fig. 8, according to the fitting of phonon vibrations by the Debye-Grüneisen model, it can be found that even though $YbFe_2Ge_2$ does not show NTE, but its thermal expansion is weakened by the single effect of valence transition. The single effect of valence transition contributes less to NTE compared with the dual effect. It needs to mention that there exists a large room to study the detailed difference between the existing single effect and the dual effect.

The present enhanced NTE in $YbMn_2Ge_2$ induced by the dual effect suggests a way to find other NTE materials, that is, to

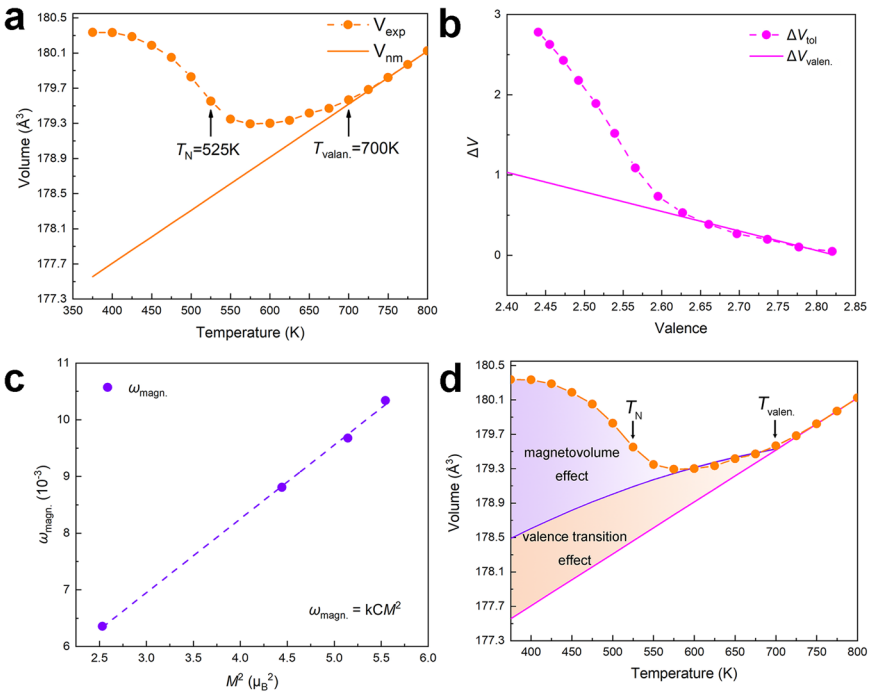

Fig. 4 The enhanced NTE induced by the dual effect. a Experimental unit cell volume (V_{exp}) determined by SXRD and nominal volume (V_{nm}) estimated from the phonon vibrations contriution. **b** Volume difference ($\Delta V_{tol} = V_{exp} - V_{nm}$) plotted as function of Yb valence and valence transition contribution ($\Delta V_{valen.}$) to NTE. **c** Correlation between M^2 and $\omega_{magn.}$. **d** The dual effect of magnetism and valence transition to the NTE of $YbMn_2Ge_2$.

construct a material containing both variable valence atoms and magnetic atoms. In addition, the dual effect is not limited to the present combination of MVE and valence transition, which can be combined in different ways through the available NTE mechanisms, such as valence transition, MVE, ferroelectricity, and low-frequency phonons. An interesting example has been found in the solid solutions of $BiNi_{1-x}Fe_xO_3$ ($0.25 \le x \le 0.5$), where NTE can be enhanced due to the simultaneous presence of valence transition and polar-to-nonpolar transition[4]. Other possible dual effect can be the combination between MVE and ferroelectricity in some multiferroics, or by combining low-frequency phonons and valence transition in some open framework structure materials. Enhanced or strong NTE can be expected, when the dual effect is exploited.

In summary, an enhanced NTE has been found out in the $YbMn_2Ge_2$ compound over a wide temperature range ($\alpha_v = -32.9 \times 10^{-6}\,K^{-1}$, $\Delta T = 175$ K). The origin of such enhanced NTE has been investigated by combining NPD and XANES measurements. As the temperature increases, the Mn moment decreases rapidly as it approaches to T_N, which leads to NTE due to the MVE. Meanwhile, the NTE is enhanced by the simultaneous valence transition of Yb from 2.40 to 2.82. These two concurrent contributions to NTE give rise to an enhanced NTE with a wide temperature range. Such dual effect, here related to magnetism and valence transition, represents an interesting opportunity to develop NTE materials.

METHODS

Sample preparation

The polycrystalline sample of $YbMn_2Ge_2$ was prepared by an arc melting under a high purity argon atmosphere. The constituent elements with 99.9% purity were used. The button sample was melted at least four times to ensure good homogenization. Then, the sample was annealed at 1223 K for five days in a quartz tube in argon atmosphere (200 mbar), and quenched quickly into cold water.

Experiment methods

The temperature dependence of SXRD data was collected at the beamline 11-ID-C of Advanced Photon Source (APS) of Argonne National Laboratory with a wavelength of $\lambda = 0.1173$ Å from 200 K to 800 K. Temperature dependence of XANEX spectra was taken at the Yb L_{III}-edge from 200 K to 700 K at the 20-BM-B beamline of APS. NPD measurements were performed on the time-of-flight (TOF) diffractometer GPPD (General Purpose Powder Diffractometer) at China Spallation Neutron Source (CSNS), Dongguan, China. The sample was loaded in the vanadium cans during the test and the NPD patterns were collected with wavelength band from 0.2 to 4.2 Å. For the NPD measurements, additional aluminum foil was wrapped outside the vanadium tube for a better temperature management.

DATA AVAILABILITY

The authors declare that the main data supporting the findings of this study are available within the paper and its supplementary information files. Extra data are available from the authors upon request.

Received: 18 November 2020; Accepted: 17 April 2021;
Published online: 14 May 2021

REFERENCES

1. Mary, T. A., Evans, J. S. O., Vogt, T. & Sleight, A. W. Negative thermal expansion from 0.3 to 1050 Kelvin in ZrW_2O_8. *Science* **272**, 90–92 (1996).
2. Chen, J. et al. Effectively control negative thermal expansion of single-phase ferroelectrics of $PbTiO_3$-(Bi, La)FeO_3 over a giant range. *Sci. Rep.* **3**, 2458 (2018).
3. Pachoud, E., Cumby, J., Lithgow, C. T. & Attfield, J. P. Charge order and negative thermal expansionin V2OPO4. *J. Am. Chem. Soc.* **140**, 636–641 (2018).
4. Nishikubo, T. et al. Enhanced negative thermal expansion induced by simultaneous charge transferand polar-nonpolar transitions. *J. Am. Chem. Soc.* **141**, 19397–19403 (2019).
5. Azuma, M. et al. Colossal negative thermal expansion in $BiNiO_3$ induced by intermetallic charge transfer. *Nat. Commun.* **2**, 1–5 (2011).
6. Huang, R. et al. Giant negative thermal expansion in $NaZn_{13}$-type $La(Fe,Si,Co)_{13}$ compounds. *J. Am. Chem. Soc.* **135**, 11469–11472 (2013).

7. Song, Y. et al. Zero thermal expansion in magnetic and metallic $Tb(Co,Fe)_2$ intermetallic compounds. *J. Am. Chem. Soc.* **140**, 602–605 (2018).
8. Greve, B. K. et al. Pronounced negative thermal expansion from a simple structure: cubic ScF_3. *J. Am. Chem. Soc.* **132**, 15496–15498 (2010).
9. Hu, L. et al. New insights into the negative thermal expansion: direct experimental evidence for the "guitar-string" effect in cubic ScF_3. *J. Am. Chem. Soc.* **138**, 8320–8323 (2016).
10. Goodwin, A. L. et al. Colossal positive and negative thermal expansion in the framework material $Ag_3[Co(CN)_6]$. *Science* **319**, 794–797 (2008).
11. Duyker, S. G. et al. Negative thermal expansion in $LnCo(CN)_6$ (Ln = La, Pr, Sm, Ho, Lu, Y): mechanisms and compositional trends. *Angew. Chem. Int. Ed.* **52**, 5266–5270 (2013).
12. Gao, Q. et al. Switching between giant positive and negative thermal expansions of a $YFe(CN)_6$-based prussian blue analogue induced by guest species. *Angew. Chem. Int. Ed.* **56**, 9023–9028 (2017).
13. Deng, S. et al. Invar-like behavior of antiperovskite $Mn_{3+x}Ni_{1-x}N$ compounds. *Chem. Mater.* **27**, 2495–2501 (2015).
14. Song, X. et al. Adjustable zero thermal expansion in antiperovskite manganese nitride. *Adv. Mater.* **23**, 4690–4694 (2011).
15. Arvanitidis, J. et al. Temperature-induced valence transition and associated lattice collapse in samarium fulleride. *Nature* **425**, 599–602 (2003).
16. Margadonna, S. et al. Valence instabilities, phase transitions, and abrupt lattice expansion at 5 K in the YbGaGe system. *J. Am. Chem. Soc.* **126**, 4498–4499 (2004).
17. Takenaka, K. et al. Giant isotropic negative thermal expansion in Y-doped samarium monosulfides by intra-atomic charge transfer. *Sci. Rep.* **9**, 1–8 (2019).
18. Long, Y. W. et al. Temperature-induced A-B intersite charge transfer in an A-site-ordered $LaCu_3Fe_4O_{12}$ perovskite. *Nature* **458**, 60–63 (2009).
19. Takenaka, K. & Takagi, H. Giant negative thermal expansion in Ge-doped anti-perovskite manganese nitrides. *Appl. Phys. Lett.* **87**, 261902 (2005).
20. Li, L. F. et al. Good comprehensive performance of Laves phase $Hf_{1-x}Ta_xFe_2$ as negative thermal expansion materials. *Acta Mater.* **161**, 258–265 (2018).
21. Pan, Z. et al. Colossal volume contraction in strong polar perovskites of Pb(Ti,V) O_3. *J. Am. Chem. Soc.* **139**, 14865–14868 (2017).
22. Pryde, A. K. et al. Rigid unit modes and the negative thermal expansion in ZrW_2O_8. *Phase Transit.* **61**, 141–153 (1997).
23. Dove, M. T., Trachenko, K. O., Tucker, M. G. & Keen, D. A. Rigid unit modes in framework structures: theory, experiment and applications. *Rev. Mineral. Geochem.* **39**, 1–33 (2000).
24. Evans, J. S. Negative thermal expansion materials. *J. Chem. Soc. Dalton Trans.* 3317-3326 (1999).
25. Hu, L. et al. Zero thermal expansion and ferromagnetism in cubic $Sc_{1-x}M_xF_3$ (M = Ga, Fe) over a wide temperature range. *J. Am. Chem. Soc.* **136**, 13566–13569 (2014).
26. Tan, J. et al. Broad negative thermal expansion operation-temperature window in antiperovskite manganese nitride with small crystallites. *Nano Res.* **8**, 2302–2307 (2015).
27. Hu, L. et al. Localized symmetry breaking for tuning thermal expansion in ScF_3 nanoscale frameworks. *J. Am. Chem. Soc.* **140**, 4477–4480 (2018).
28. Gao, Q. et al. Tunable thermal expansion from negative, zero, to positive in cubic prussian blue analogues of $GaFe(CN)_6$. *Inorg. Chem.* **57**, 14027–14030 (2018).
29. Hofmann, M. et al. Valence and magnetic transitions in $YbMn_2Ge_2$-pressure and temperature. *Phys. B* **385**, 330–332 (2006).
30. Hofmann, M., Campbell, S. J. & Edge, A. V. J. Valence and magnetic transitions in $YbMn_2Si_{2-x}Ge_x$. *Appl. Phys. A* **74**, s713–s715 (2002).
31. Hofmann, M., Campbell, S. J. & Szytula, A. Antiferromagnetism in $YbMn_2Ge_2$–Mn magnetic sublattice. *J. Alloy Compd* **311**, 137–142 (2000).
32. Morellon, L. et al. The magnetic phase transitions and related volume changes in $(Nd_{1-x}Tb_x)$ Mn_2Ge_2 compounds. *J. Magn. Magn. Mater.* **177**, 1085–1086 (1998).
33. Morellon, L., Algarabel, P. A., Ibarra, M. R. & Ritter, C. Magnetic structures and magnetic phase diagram of $Nd_xTb_{1-x}Mn_2Ge_2$. *Phys. Rev. B* **55**, 12363–12374 (1997).
34. Guillaume, C. É. Recherches sur les aciers au nickel. Dilatations aux temperatures elevees; resistance electrique. *CR Acad. Sci.* **125**, 235–238 (1897).
35. Mazet, T., Welter, R. & Malaman, B. A study of the new ferromagnetic $YbMn_6Sn_6$ compound by magnetization and neutron diffraction measurements. *J. Magn. Magn. Mater.* **204**, 11–19 (1999).
36. Pöttgen, R. et al. The stannides YbPtSn and $Yb_2Pt_3Sn_5$. *Z. Kristallogr.* **214**, 143–150 (1999).
37. Di Napoli, S., Llois, A. M., Bihlmayer, G. & Blügel, S. Magnetic order in RMn_2Ge_2 (R = Y, Ca) compounds and their solid solutions with $LaMn_2Ge_2$. *Phys. Rev. B* **75**, 104406 (2007).
38. Venturini, G., Welter, R., Ressouche, E. & Malaman, B. Neutron diffraction study of the ferromagnetic to antiferromagnetic transition in $La_{0.3}Y_{0.7}Mn_2Ge_2$: phenomenological description of the magnetic behaviour of Mn in $ThCr_2Si_2$ silicides and germanides. *J. Alloy. Compd* **223**, 101–110 (1995).
39. Hofmann, M., Campbell, S. J., Edge, A. V. J. & Studer, A. J. The magnetic structures of $YbMn_2Si_2$. *J. Phys. Condens. Matter* **13**, 9773–9780 (2001).
40. Szytuła, A. & Szott, I. Magnetic properties of ternary RMn_2Si_2 and RMn_2Ge_2 compounds. *Solid State Commun.* **40**, 199–202 (1981).
41. Venturini, G., Welter, R., Ressouche, E. & Malaman, B. Neutron diffraction study of $Nd_{0.35}La_{0.65}Mn_2Si_2$: a $SmMn_2Ge_2$-like magnetic behaviour compound. *J. Magn. Magn. Mater.* **150**, 197–212 (1995).
42. Temmerman, W. M. et al. Electronic configuration of Yb compounds. *Phys. Rev. Lett.* **83**, 3900–3903 (1999).
43. Bauer, E.D. et al. Pressure-induced valence change in $YbAl_3$: a combined high pressure inelastic x-ray scattering and theoretical investigation. *Phys. Rev. B* **78**, 75117 (2008).
44. Margadonna, S., Arvanitidis, J., Papagelis, K. & Prassides, K. Negative thermal expansion in the mixed valence ytterbium fulleride, $Yb_{2.75}C_{60}$. *Chem. Mater.* **17**, 4474–4478 (2005).
45. Jiang, W. B. et al. Crossover from a heavy fermion to intermediate valence state in noncentrosymmetric $Yb_2Ni_{12}(P,As)_7$. *Sci. Rep.* **5**, 17608 (2015).
46. Bauer, E. et al. Evolution of a magnetic state in $YbCu_{5-x}Ga_x$. *Phys. Rev. B* **52**, 4327–4335 (1995).
47. Kumar, R. S. et al. Pressure-induced valence and structural changes in $YbMn_2Ge_2$-inelastic X-ray spectroscopy and theoretical investigations. *Inorg. Chem.* **52**, 832–839 (2013).
48. Grüneisen, E. Handbuch der Physik, 10, 22 (1926). *Ann. Phys.* **39**, 258 (1912).
49. Sayetat, F., Fertey, P. & Kessler, M. An easy method for the determination of Debye temperature from thermal expansion analyses. *J. Appl. Crystallogr.* **31**, 121–127 (1998).
50. Cornelius, A. L. et al. Experimental studies of the phase transition in $YbIn_{1-x}Ag_xCu_4$. *Phys. Rev. B* **56**, 7993–8000 (1997).
51. Moriya, T. & Usami, K. Magneto-volume effect and invar phenomena in ferromagnetic metals. *Solid State Commun.* **34**, 95–99 (1980).
52. Fujita, A., Fukamichi, K., Wang, J. T. & Kawazoe, Y. Large magnetovolume effects and band structure of itinerant-electron metamagnetic $La(Fe_xSi_{1-x})_{13}$ compounds. *Phys. Rev. B* **68**, 104431 (2003).
53. Takenaka, K. et al. Magnetovolume effects in manganese nitrides with anti-perovskite structure. *Sci. Technol. Adv. Mater.* **15**, 15009 (2014).
54. Felner, I. et al. Ytterbium valence phase transition in $Yb_xIn_{1-x}Cu_2$. *Phys. Rev. B* **35**, 6956–6963 (1987).
55. Hofmann, M., Campbell, S. J. & Edge, A. V. J. $EuMn_2Ge_2$ and $EuMn_2Si_2$: Magnetic structures and valence transitions. *Phys. Rev. B* **69**, 174432 (2004).
56. Kolmakova, N. P., Sidorenko, A. A. & Levitin, R. Z. Features of the magnetic properties of rare-earth intermetallides RMn_2Ge_2 (Review). *Low Temp. Phys.* **28**, 653–668 (2002).
57. Venturini, G. et al. Magnetic properties of $DyMn_2Ge_2$ from Mossbauer and neutron-diffraction studies. *Phys. Rev. B* **46**, 207–216 (1992).

ACKNOWLEDGEMENTS

This work was supported by the National Natural Science Foundation of China (grant nos. 21825102, 22090042, and 22075014), and the Fundamental Research Funds for the Central Universities, China (grant nos. FRF-TP-18-001C2, 06500162 and 06500201). This research used resources of the Advanced Photon Source, a U.S. Department of Energy (DOE) Office of Science User Facility operated for the DOE Office of Science by Argonne National Laboratory under Contract No. DE-AC02-06CH11357. We highly appreciate Dr. Yang Ren for the help in collecting the temperature dependence of SXRD data at the beamline 11-ID-C of APS.

AUTHOR CONTRIBUTIONS

J.C. and Y.Q.Q. conceived this study and designed the experiments. Y.Q.Q. carried out the experiments of sample preparation. L.L.F. collected the data of SXRD and XANES. A.S. analyzed the data of XANES. Y.Q.Q. and L.H.H. collected the data of NPD. Y.Q.Q. and Y.Z.S. analyzed the data of NPD. Y.Q.Q., A.S., Q.S., S.X.H., and J.C. analyzed the contribution of dual effect to NTE. J.C., X.R.X., and H.J.Z. guided the projects. All authors discussed the results and commented on the manuscript.

COMPETING INTERESTS

The authors declare no competing interests.

ADDITIONAL INFORMATION

Supplementary information The online version contains supplementary material available at https://doi.org/10.1038/s41535-021-00348-z.

Correspondence and requests for materials should be addressed to J.C.

Reprints and permission information is available at http://www.nature.com/reprints